Received: 1 January 2018 | Accepted: 7 July 2019

DOI: 10.1002/hyp.13554

SPECIAL ISSUE: WATER IN THE CRITICAL ZONE

WILEY

Catchment chemostasis revisited: Water quality responds differently to variations in weather and climate

Sarah E. Godsey[1] | Jens Hartmann[2] | James W. Kirchner[3,4,5]

[1]Department of Geosciences, Idaho State University, Pocatello, ID

[2]Institute for Geology, Center for Earth System Research and Sustainability (CEN), Universität Hamburg, Hamburg, Germany

[3]Department of Environmental Systems Science, ETH Zurich, Zurich, Switzerland

[4]Swiss Federal Research Institute WSL, Birmensdorf, Switzerland

[5]Department of Earth and Planetary Science, University of California, Berkeley, Berkeley, CA

Correspondence
Sarah E. Godsey, Idaho State University, Pocatello, ID.
Email: godsey@isu.edu

01
cholas Gubbins

02
cholas Gubbins

Abstract

Solute concentrations in streamflow typically vary systematically with stream discharge, and the resulting concentration–discharge relationships are important signatures of catchment biogeochemical processes. Solutes derived from mineral weathering often exhibit decreasing concentrations with increasing flows, suggesting dilution of a kinetically limited weathering flux by a variable flux of water. However, previous work showed that concentration–discharge relationships of weathering-derived solutes in 59 headwater catchments were much weaker than this simple dilution model would predict. Instead, catchments behaved as chemostats, with rates of solute production and/or mobilization that were nearly proportional to water fluxes, on both event and interannual timescales. Here, we re-examine these findings using data for a wider range of solutes from 2,186 catchments, ranging from ~10 to >1,000,000 km^2 in drainage area and spanning a wide range of lithologic and climatic settings. Concentration–discharge relationships among this much larger set of larger catchments are broadly consistent with the previously described chemostatic behaviour, at least on event and interannual timescales for weathering-derived solutes. Among these same catchments, however, site-to-site variations in mean concentrations of weathering-derived solutes exhibit strong negative correlations with long-term average precipitation and discharge, reflecting strong climatic control on long-term leaching of the critical zone. We use multiple regression of site characteristics including discharge to identify potential controls on long-term mean concentrations and find that lithologic and land cover controls are significant predictors for many analytes. The picture that emerges is one in which, on event and interannual timescales, weathering-derived stream solute concentrations are chemostatically buffered by groundwater storage and fast chemical reactions, but each catchment's chemostatic "set point" reflects site-to-site differences in climatically driven evolution of the critical zone. In contrast to these weathering products, some nutrients and particulates are often near-chemostatic across all timescales, and their long-term mean concentrations correlate more strongly with land use than climatic characteristics.

KEYWORDS

chemostasis, climate–weathering feedback, concentration–discharge, dissolved load, water quality

1 | INTRODUCTION

Temporal patterns of solute concentrations during and between hydrological events reflect a combination of delivery, storage, and reaction processes (Hem, 1985; Johnson, Likens, Bormann, Fisher, & Pierce, 1969) and can be used to assess or predict water quality and pollutant remediation across catchments (House & Warwick, 1998; Walling & Webb, 1986). Concentration–discharge (*C*–*Q*) relationships are widely used in conjunction with other analyses to compute solute loads (e.g., Aulenbach & Hooper, 2006; Basu et al., 2010), biogeochemical mass balances (e.g., Hall, 1970; Pinder & Jones, 1969), and long-term rates of chemical weathering (and, by extension, geochemical uptake of atmospheric carbon dioxide; e.g., Berner, Lasaga, & Garrels, 1983; Kump, Brantley, & Arthur, 2000; Maher & Chamberlain, 2014). Previous work on these relationships has shown that concentrations of weathering-derived solutes in streamflow remain nearly chemostatic across wide ranges of discharge in a broad sample of U.S. watersheds (e.g., Godsey, Kirchner, & Clow, 2009). The stability of these solute concentrations despite changes in flow reflects the catchment system's set point (*sensu* systems control theory)—the value around which negative feedbacks act to maintain an approximate equilibrium. However, different sites and solutes exhibit different set point concentrations (Godsey et al., 2009; Moon, Chamberlain, & Hilley, 2014), and it is unclear how much these set points vary due to climatically driven geochemical evolution of the critical zone.

Widely varying *C*–*Q* patterns have been observed for different solutes. For example, although concentrations have been observed to remain nearly constant for some solutes derived from geochemical weathering, and for biogenic solutes with large legacies or reservoirs (e.g., Basu et al., 2010), they can vary more dramatically for other nutrients (Herndon et al., 2015). Suspended sediment has also been examined in the *C*–*Q* context, although the physics of sediment transport clearly differs from the mechanisms that control solute concentrations. There is one key aspect, however, that is similar: supply limitations in both sediments and solutes can affect *C*–*Q* patterns, especially during prolonged high flows (Rose, Karwan, & Godsey, 2018).

Individual solutes can exhibit different degrees of chemostasis in different watersheds, reflecting a suite of drivers including climate, lithology, scale, human management, and stream intermittency (e.g., Creed et al., 2015; Hale & Godsey, 2019; Moatar, Abbott, Minaudo, Curie, & Pinay, 2017; Stallard & Murphy, 2014). Decades of chemical weathering studies have used watershed flux data to document lithologic and climatic controls on river solute concentrations (e.g., Bluth & Kump, 1994; Gaillardet, Dupre, Louvat, & Allegre, 1999; Ibarra et al., 2016; Meybeck, 1987; West, Galy, & Bickle, 2005), and understanding *C*–*Q* relationships may illuminate weathering–climate feedbacks (Moon et al., 2014). Many possible mechanisms have been invoked to explain observed *C*–*Q* patterns (e.g., Lloyd, Freer, Johnes, & Collins, 2016a, 2016b; Musolff, Fleckenstein, Rao, & Jawitz, 2017). These mechanisms usually rely on assumptions about the storage volume in the watershed, the surface area that is available to react (e.g., White et al., 1996), and rates of solute production, mobilization, and mixing, often expressed by the ratio of mean transit time to reaction time, known as the Damköhler number (Ibarra et al., 2016; Ibarra, Moon, Caves, Chamberlain, & Maher, 2017; Maher, 2011; Maher & Chamberlain, 2014). The Damköhler number reflects the relative efficiency of reaction kinetics (including metabolic reaction limits) versus storage and transport in shaping solute concentrations. Available surface areas, secondary mineral interactions, and flushing volumes or rates are likely to vary with changes in dominant flowpaths, including shifts from groundwater to shallow soil flowpaths (e.g., Tardy, Bustillo, & Boeglin, 2004). Weather and climate may influence these flowpaths through changes in precipitation patterns and may partially control reaction kinetics through variations in wetted surface area, through variations in rainfall chemistry, and through the temperature dependence of reaction rates.

The effects of climatic variations may differ across different timescales; for example, increased flushing rates on event or interannual timescales may lead to higher solute fluxes and nearly chemostatic concentrations, whereas under long-term kinetic limitations, higher flushing rates may imply greater depletion of labile geochemical storages and thus lower solute concentrations (assuming that rainfall is not the dominant solute source). In some cases, large decreases in solute fluxes have been documented or inferred from changes in soil profile weathering over 10-ka timescales (e.g., Börker, Hartmann, Romero-Mujalli, & Li, 2019; Taylor & Blum, 1995). Although these contrasting climatic controls could potentially be observable in *C*–*Q* comparisons spanning multiple temporal scales, most analyses typically focus on event timescales and sometimes on interannual timescales. Although the longer-term implications of these analyses are often assumed, they are not explicitly analysed because *C*–*Q* data are simply not available on timescales of centuries or millennia.

Instead, long-term solute production from mineral weathering has often been inferred from chronosequence studies that compare soil composition across different parent material ages (e.g., Porder, Hilley, & Chadwick, 2007; Taylor & Blum, 1995). Chronosequence studies assume that the short-term dynamics at a given site are small compared with the cumulative effects of long-term trends and that within-site spatial heterogeneity can be accounted for or is minimal compared with long-term patterns (Pickett, 1989). Alternatively, the long-term effects of climate (and other controls) have been studied by comparing contemporary solute fluxes across multiple contrasting watersheds (Bluth & Kump, 1994; Gaillardet et al., 1999; Hilley & Porder, 2008; Oliva, Viers, & Dupré, 2003; West et al., 2005; White & Blum, 1995). Watershed comparisons typically rely on solute and site data compiled from a few dozen catchments to test the importance of a specific hypothesized control, such as lithology, precipitation, runoff, vegetation, physical erosion, or soil characteristics, without necessarily knowing how long these conditions have prevailed at each watershed. Instead, differences in these hypothesized key controls are assumed to drive any differences in solute fluxes. Site characteristics that are not accounted for can compromise the inferences from these

watershed. Here, we attempt to address the limitations of these catchment comparison studies in two ways: (a) comparing solute patterns across many more sites than are typically assessed and (b) building a model that explicitly accounts for as many factors as possible. Here, we use compiled global river chemistry data (Hartmann, Lauerwald, & Moosdorf, 2014) to evaluate whether previously observed chemostatic patterns of weathering-derived solutes at well-studied sites across the United States also hold for a much larger set of basins and a much wider range of solutes. These new data also allow us to compare long-term average solute concentrations from site to site across climatic gradients to determine how catchments' chemostatic set points vary in response to climatically driven geochemical evolution of the critical zone.

2 | METHODS

We analysed *C*–*Q* patterns in hydrochemical data from the GLORICH database. For documentation of the GLORICH database itself, we direct readers to the original publication (Hartmann et al., 2014); here, we will focus on outlining its advantages and disadvantages for global *C*–*Q* analysis. The most obvious advantage of this database is its size and global coverage. However, except for a subset of primarily North American and European sites, stream discharges in the GLORICH database are primarily modeled rather than measured. Modeled flows can be useful for many purposes (such as deriving flux estimates), but modeling choices can strongly affect the inferred *C*–*Q* relationships, even that discharge is the independent variable of interest.

03 Nicholas Gubbins

04 Nicholas Gubbins

To minimize this risk, we evaluated *C*–*Q* relationships only for sites where measured discharges were available. To augment GLORICH's measured streamflows, we replaced the modeled Canadian streamflows in the database with instrumental measurements, using Environment Canada records for the closest gauging station (within 3 km of the recorded sampling location) whenever possible. Thus, for some of these sites, flow data may be inferred from nearby flow measurements, which may not exactly reflect the flow conditions at the sampling point (Oudin, Andreassian, Perrin, Michel, & Le Moine, 2008). Nonetheless, on the basis of a review of *C*–*Q* patterns, discharge records, and discharge–area plots, we believe that, for this analysis, the measured values present more useful estimates of flow conditions than the original modeled discharges in GLORICH.

As may be expected from such a large database, data are occasionally missing and sampling may be erratic. Because of these limitations, some sites have too little variation in the available flow data to assess the *C*–*Q* relationship. After culling out such sites on the basis of the specific criteria outlined below, we restricted our analyses to the ~2,000 locations where sufficient measured flows were available rather than relying on modeled flows.

We analysed relationships between concentration and discharge at the event timescale and the interannual timescale; we also analysed the relationship between long-term average concentrations and discharges from site to site. At the event scale, we plotted concentrations of all available solutes against area-normalized instantaneous discharge (both on logarithmic scales) at each site for each sample. We restricted our analysis to GLORICH's "single" sampling mode rather than including composite samples (for which instantaneous discharge might be hard to assess) and to sites where at least 20 samples were available. These total 2,186 sites, over half of which (1,122) are in the United States, with smaller contributions from Australia (277), Canada (266), the United Kingdom (266), Germany (162), and Spain (78); the remaining 15 sites are distributed among six other countries. We also restricted the analysis to site/analyte combinations where at least half of the concentrations were not identical, where there was non-zero variance in flow, and where the R^2 was <.999 (to exclude cases where concentration values had obviously been calculated from an assumed *C*–*Q* relationship). To focus our analysis on sites with meaningful log–log slopes, we also excluded site/analyte combinations for which the standard error of the slope exceeded 0.1. These criteria excluded ~100 potential sites from this analysis. We then summarized the resulting slopes and their uncertainties, in a manner similar to our previous work for the 59 U.S. Geological Survey Hydrological Benchmark Network sites (Godsey et al., 2009).

We also performed similar *C*–*Q* analyses at the interannual timescale, plotting flow-weighted mean annual concentrations against mean annual discharge. Here, our analysis was restricted to 1,189 U.S. and Canadian sites, for which we could obtain reasonably complete daily discharge records. For our interannual analysis, we determined mean annual discharge only for sites and years for which at least 350 days of discharge data were available, and we calculated volume-weighted mean concentrations for sites, years, and solutes for which at least four samples were available. We then calculated the log–log slopes of the annual flow-weighted means as functions of the annual total discharges, for all sites and analytes for which at least eight water years of concentration and discharge data were available. Interannual *C*–*Q* slopes were included in further analysis if their standard errors were less than 0.2, double the uncertainty threshold permitted for the event-scale analysis. Changing these data inclusion thresholds had little effect on our results. For example, restricting our analyses to only sites with 20 years of annual data reduced the number of valid sites for our interannual Ca^{2+}–Q analysis by a factor of ~2 but changed the average estimated slope by only 2%.

We also compared long-term average concentrations and flows across sites, as a measure of how site-to-site climatic differences have shaped the chemostatic set points that anchor shorter-term *C*–*Q* patterns. For this analysis, we calculated the mean flow-weighted concentration for each solute (again focusing on the 1,189 U.S. and Canadian sites for which we could obtain reasonably complete discharge data), excluding samples that lacked accompanying discharge measurements. We then log transformed the mean concentrations and mean discharge of each site, excluding all site/analyte combinations with fewer than 20 samples. We then determined site-to-site relationships between average concentrations and average discharge in two distinct ways.

First, for each solute, we calculated the log–log slope of a scatterplot of long-term mean concentration against long-term mean discharge, with one point for each site where these values could be calculated. Because many solutes exhibited different behaviour across humid and arid sites, we calculated these long-term site-to-site slopes for arid and humid sites separately in a piecewise fashion. We used a threshold mean streamflow of 15 cm year^{-1} (0.4 mm day^{-1}) to separate catchments into arid and humid sites. (This approach echoes Molnar et al.'s 2017 separation of *C*–*Q* relationships into high and low flows at individual sites.) We call these the "uncorrected" site-to-site *C*–*Q* slopes.

Second, because these site-to-site relationships between long-term average stream chemistry and long-term mean discharge could potentially be obscured or distorted by site-to-site variations in other site characteristics (such as lithology and land use), we corrected for these potentially confounding factors by constructing multiple regression models with long-term discharge and the following catchment characteristics from the GLORICH database:

- drainage area (log transformed)
- average catchment slope (log transformed)
- average dust deposition (Mahowald et al., 2005; log transformed)
- Moderate Resolution Imaging Spectroradiometer (MODIS) net primary productivity (g C m^{-2} a^{-1}; Zhao, Heinsch, Nemani, & Running, 2005)
- WorldClim annual average temperature (°C; Hijmans, Cameron, Parra, Jones, & Jarvis, 2005)
- fraction of catchment underlain by carbonate rocks (sum of the global lithological map [GLiM] categories sc and sm; Hartmann & Moosdorf, 2012)
- fraction of catchment underlain by magmatic rocks (sum of GLiM categories va, vb, vi, pa, pb, py, and pi)
- fraction of catchment underlain by siliciclastic rocks (GLiM category ss)
- fraction of catchment underlain by metamorphic rocks (GLiM category mt)
- fraction of urban land use (GlobCover; Arino et al., 2007)
- fraction of managed agricultural land (GlobCover)
- fraction of forest cover (GlobCover)
- fraction of open water and wetland (GlobCover)

We also included terms for the logarithm of long-term average discharge (again separated into two groups by the humid/arid threshold of 15 cm year^{-1}) and an additional constant (i.e., intercept) to account for any additive offset between humid versus arid sites. Models were selected by an automated stepwise elimination procedure ("backward" selection) using a minimum Bayesian Information criterion. That is, we included all possible terms and removed them one at a time, replacing them if the model prediction was much worse than one might expect by a model with one fewer parameter and retaining only the strongest predictor variables. If the discharge terms were eliminated by this procedure, they were manually added back in, because we are interested in the discharge dependence of solute concentrations even when discharge is a poor explanatory variable (i.e., chemostatic behaviour). These discharge terms are the "site-characteristic-corrected" values reported and discussed below. They are analogous to the uncorrected simple linear regression slopes and would be numerically identical to them if none of the other site characteristics mentioned above were confounding. Both the "corrected" and "uncorrected" slopes reflect how much one might expect the long-term average concentration of a particular solute to change as the long-term average discharge changes. In other words, the discharge term reveals the possible role of climate variations on the chemical set points of individual catchments. We report both uncorrected and corrected values below, because they both reveal possible controls on watershed-scale chemical weathering. All calculations were performed in JMP 13.1.0 (SAS Institute, Inc., Cary, NC, USA).

3 | RESULTS

Both the event and interannual *C*–*Q* slopes for weathering-derived solutes are broadly similar to those found in our previous work at a much smaller set of sites (Godsey et al., 2009). At both event timescales (Figure 1a) and interannual timescales (Figure 1b), concentrations of weathering-derived solutes vary much less than discharge does. Thus the best fit log–log *C*–*Q* relationships are much shallower than the slope of −1 that would be expected for simple dilution (example distributions of slopes for potassium and magnesium are shown in Figure 2).

By contrast, plots of long-term average concentration against long-term average discharge across different sites have steeper slopes that vary from one solute to the next, with site-to-site scatterplots often forming broad clouds that lie parallel to the simple dilution (C~1/Q) diagonal line, especially for more humid sites (e.g., Figure 1c). If we plot the normalized probability distribution curves for event and interannual *C*–*Q* slopes on event and interannual timescales for all sites (light and dark blue curves, Figure 2) and compare them with the corrected humid and arid long-term intersite *C*–*Q* slopes, we see that the humid long-term site-to-site slope (green line, Figure 2) is typically significantly steeper (more negative) than most of the event and interannual slopes for the same solutes and the arid long-term site-to-site slope (orange line, Figure 2) is also slightly steeper.

The log-transformed *C*–*Q* plots showing intersite comparisons of long-term average flows and concentrations (Figure 1c) exhibit non-linear relationships for both potassium and magnesium, with an apparent slope break between humid and arid sites. Power-law slopes for humid sites are often steeper than those for arid sites (as summarized in Figure 3b,c).

The analysis presented here extends beyond base cations and anions to include nutrients, suspended sediment, and carbon species. The *C*–*Q* relationships depicted in Figures 1 and 2 for potassium and magnesium are summarized across all analytes, sites, and timescales in Figure 3. This summary shows that the log–log *C*–*Q* slopes are generally steeper (i.e., closer to −1) in the intersite

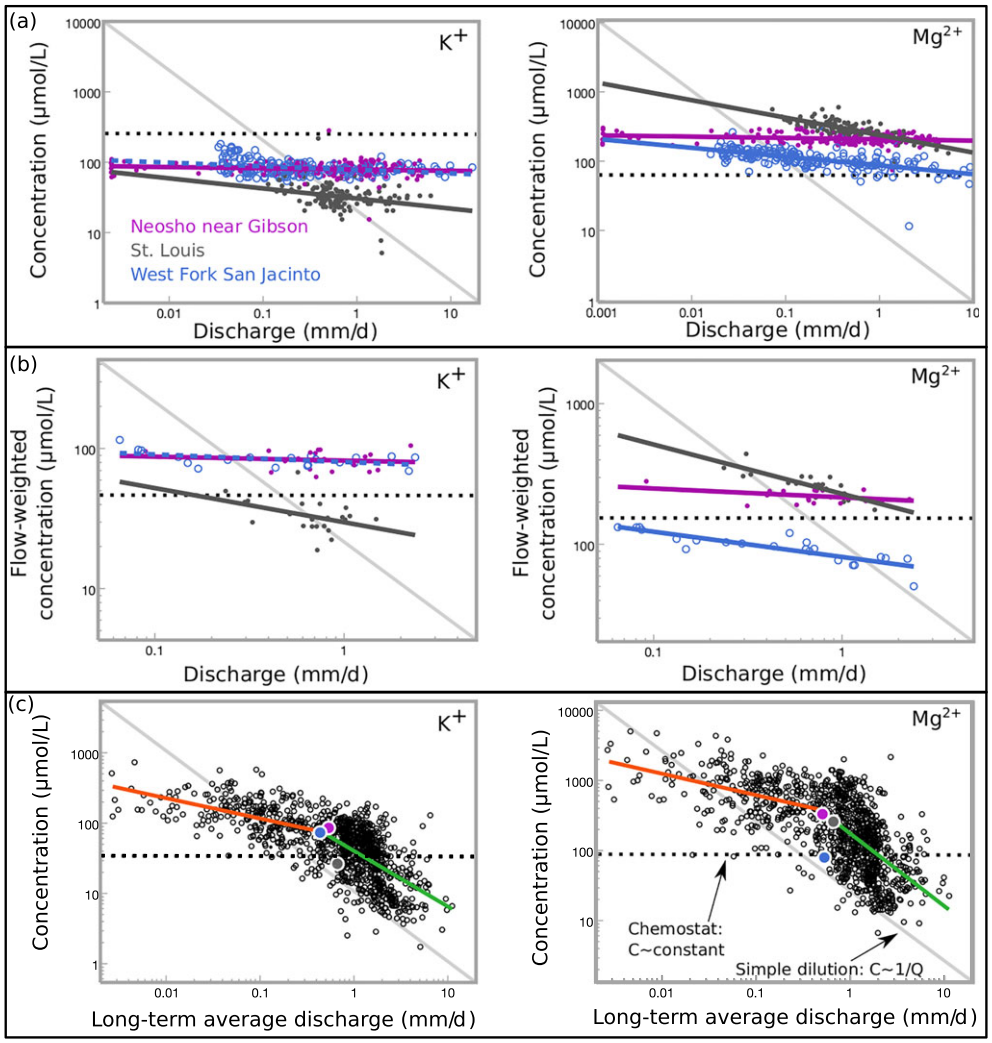

FIGURE 1 Concentration–discharge (*C*–*Q*) relationships on event (a) and interannual (b) timescales at individual sites, compared with site-to-site relationships between long-term mean *C* and long-term mean *Q* across many sites (c), for potassium (left column), and magnesium (right column). The event and interannual slopes are close to 0, indicating that these [illegible]s are nearly chemostatic at [illegible] short timescales. The slopes grow slightly steeper from (a) to (b), indicating slightly stronger dilution behaviour at longer timescales. By contrast, the site-to-site relationships between long-term mean concentrations and discharges (c), reflecting *C*–*Q* relationships across climatic gradients, are much steeper. The three sites shown in (a) and (b) are indicated by same-coloured dots in (c). Separate best-fit lines are shown for arid (orange) and humid (green) sites in (c), illustrating the markedly steeper intersite *C*–*Q* relationships among the humid sites. No site-characteristic corrections (see Section 2) are applied in (c); instead, the uncorrected slopes in (c) can be directly compared with the corrected slopes shown for parameters "arid_log_q" and "humid_log_q" under the appropriate solute column in Table 1

comparisons, but the patterns are not always consistent (compare Figure 3b,c with Figure 3a). The *C*–*Q* slopes are also more variable in the intersite comparisons, as indicated by the error bars (which depict standard errors of means, where these are larger than the plotting symbols).

Here, we summarize the general patterns observed for the different solute groups in Figure 3, as well as the exceptions to those patterns. Importantly, Figures 3b and 3c both show slopes of long-term mean concentration versus long-term mean discharge across many sites, but they differ in one key respect: only Figure 3c is corrected for the influence of other site characteristics, using the multiple regression approach outlined in the Section 2. We present both uncorrected and corrected results throughout this section to highlight the role of discharge and other site characteristics in controlling long-term mean concentrations.

Base cations (Ca^{2+}, Mg^{2+}, Na^{+}, K^{+}, and Sr^{2+}) exhibit nearly chemostatic to weakly diluting behaviour over event and interannual timescales represented by the *C*–*Q* patterns at individual sites, whereas in the intersite comparison, they usually exhibit strong dilution (*C*–*Q* slopes between −0.5 and −1) across humid sites and weak dilution across arid sites. One clear exception to this behaviour is sodium, which exhibits weakly diluting behaviour across both arid and humid sites. Anions (Cl^{-}, F^{-}, and SO_4^{2-}) are nearly chemostatic on both event and interannual timescales, and in the intersite comparison, they are typically moderately diluting across both arid and humid sites. Another clear exception to this pattern is Cl^{-}, which exhibits

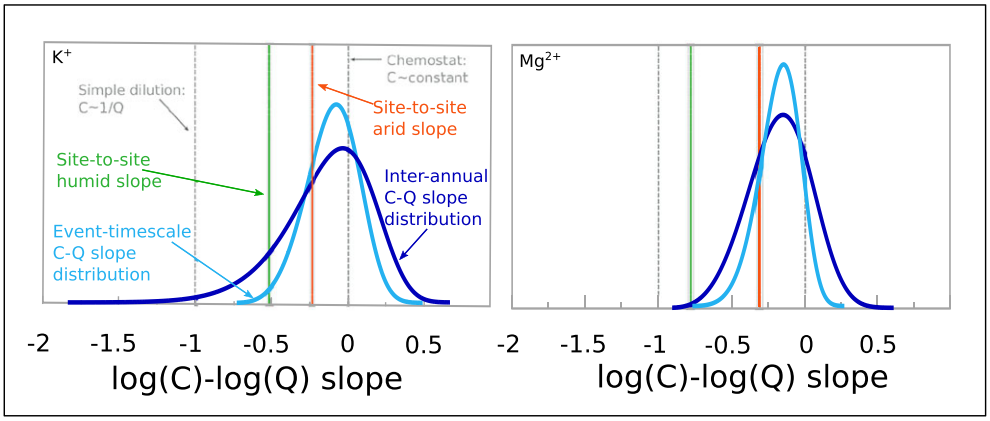

FIGURE 2 Normalized frequency distributions of log *C*–log *Q* slopes for potassium and magnesium across all sites at the event (light blue curve) and interannual (dark blue curve) timescales, compared with site-to-site *C*–*Q* slopes across the humid (green vertical line) and arid (orange vertical line) sites, corrected for potentially confounding site characteristics. Normalization is performed simply by ensuring that the area under each Weibull distribution sums to 100% of the observations available at the given timescale. The grey bands around the orange and green lines reflect the uncertainty in the best fit slope of the site-to-site *C*–*Q* relationships

different behaviour depending on whether the relationship is corrected for site characteristics (Figure 3b vs. 3c). Site characteristics apart from discharge account for much of the variability in long-term mean Cl^- at humid sites, such that Cl^- does not vary systematically with discharge across humid sites when other site characteristics are considered (Figure 3c). Consistent with the overall pattern of base cations and anions, specific conductivity (SpecCond in Figure 3) also exhibits near chemostatic to weakly diluting behaviour that is nearly identical at both event and interannual timescales; in the intersite comparison, the behaviour is weakly to moderately diluting, depending on whether the sites are more arid or humid.

The carbon, nitrogen, and phosphorus species exhibit more complex patterns at all timescales. At event timescales, carbonate and bicarbonate (representing alkalinity counterbalanced by major base cations) show weakly diluting behaviour whereas DOC, POC, and TOC (dissolved, particulate, and total organic carbon) all exhibit weakly concentrating or chemostatic behaviour. Only carbonate and POC shift from event to interannual timescales, both showing a decreasing slope with weakly to moderately diluting behaviour for carbonate and weakly concentrating to near-chemostatic behaviour for POC. In the intersite comparison, only arid sites' carbonate patterns exhibit weakly concentrating behaviour and only do so when site characteristic corrections are not applied (Figure 3b), whereas all other carbon species' slopes exhibit near-chemostatic or diluting behaviour across both humid and arid sites (Figure 3b,c). Only carbonate exhibits strong dilution behaviour and only across humid sites, and only POC exhibits more chemostatic behaviour across humid sites than across arid ones. Bicarbonate exhibits strong-to-moderate dilution behaviour across humid sites, depending on whether site characteristic corrections are applied.

At the event timescale, all N species exhibit near-chemostatic to slightly concentrating behaviour, whereas at the interannual timescale, nearly all N species are chemostatic except for DKN (dissolved Kjeldahl nitrogen), which exhibits weakly diluting behaviour. In the intersite comparison, with no correction for site characteristics, weak-to-moderate dilution behaviour is common for most N species, except for DN (dissolved N), which is chemostatic across arid sites and moderately diluting across humid sites. However, with corrections for site characteristics, only DN, TKN (total Kjeldahl nitrogen), and TN (total N) exhibit weakly to moderately diluting behaviour across humid sites and only TN and TKN exhibit weakly diluting behaviour across arid sites. All other N species exhibit near-chemostatic behaviour. When no site characteristic correction is applied, only TNH_4 (total ammonia) and TKN exhibit no significant difference in behaviour between humid and arid sites; most other N species exhibit significantly stronger dilution behaviour for the humid sites (Figure 3b). However, when site characteristic corrections are applied, only DN and TN exhibit more dilution-like behaviour across humid sites, whereas only DNH_4 exhibits more near-chemostatic behaviour across humid sites (Figure 3c). All other N species exhibit similar behaviour across both humid and arid sites.

Phosphorus species exhibit nearly identical behaviour at both the event and interannual timescales, with near chemostasis observed for DIP and DP (dissolved inorganic P and dissolved P), and slightly concentrating behaviour observed for TP (total P). In the intersite comparison, significant differences exist between arid and humid sites (Figure 3b,c): arid sites remain nearly chemostatic for DIP and DP and weakly diluting for total P, whereas humid sites are weakly to strongly diluting for all P species, depending on site-characteristic corrections and species.

SiO_2 differs from all other weathering-derived solutes in this analysis: it is nearly chemostatic across all timescales and also in the intersite comparisons. This distinct pattern is particularly important to note because many reactive transport models focus on SiO_2 (e.g., Maher & Chamberlain, 2014). Unlike many other solutes, SiO_2 exhibits only a slight difference in site-to-site slope between the arid and

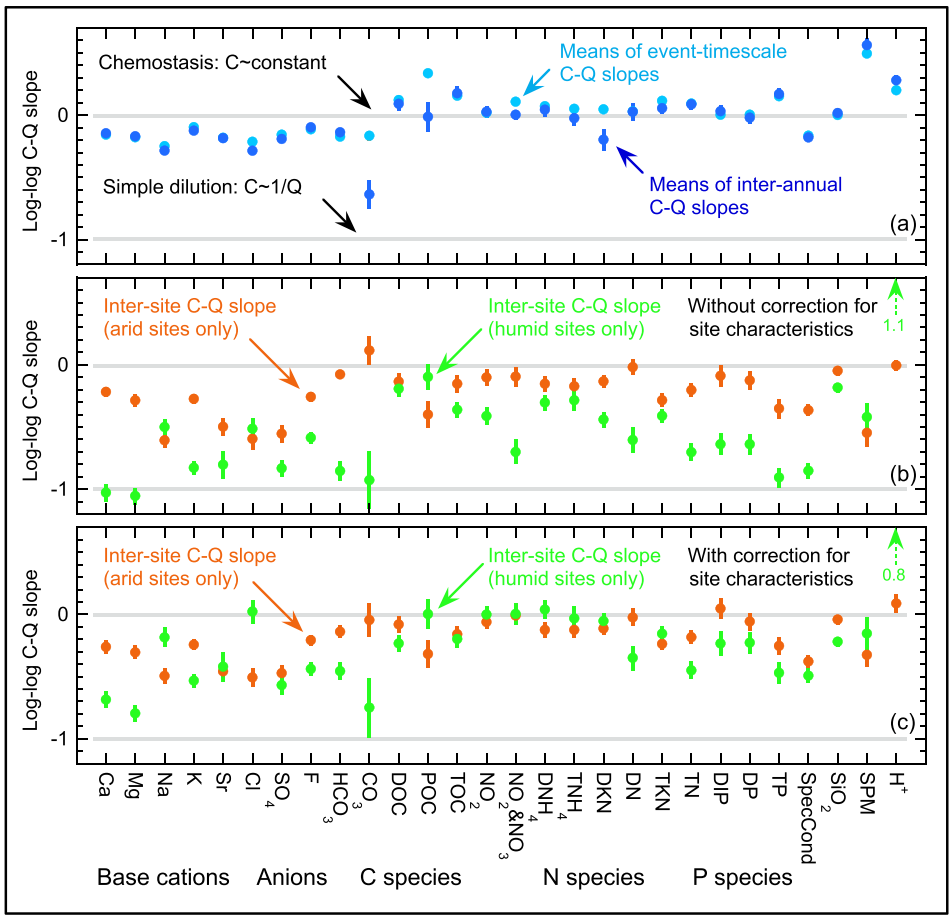

FIGURE 3 Slopes of the best-fit lines for scatterplots like those shown in Figure 1 can be summarized across all analyte/site combinations: (a) mean log *C*–log *Q* slopes for event (light blue) and interannual (dark blue) timescales for multiple solutes; (b) mean intersite log *C*–log *Q* slopes across arid sites (orange, average runoff <0.4 mm day^{-1} = 15 cm year^{-1}) and humid sites (green, average runoff >0.4 mm day^{-1}) without accounting for site characteristics; and (c) mean intersite log *C*–log *Q* slopes across arid sites (orange, average runoff <0.4 mm day^{-1}) and humid sites (green, average runoff >0.4 mm day^{-1}) after accounting for site characteristics. Event and interannual *C*–*Q* slopes are generally closer to 0 (a) than intersite *C*–*Q* slopes are (b), indicating that near-chemostatic *C*–*Q* relationships are less likely to hold across climatic gradients. Humid sites often have steeper slopes than arid sites, but these differences typically become smaller when other site characteristics are also taken into account (b vs. c) through multiple linear regression (see Table 1). Error bars indicate the standard errors of the mean slopes and are smaller than the plotting symbols in many cases. Analytes are broadly sorted into weathering-derived solutes, biologically active species, and general water quality parameters across the horizontal axis. DOC, POC, and TOC are dissolved, particulate, and total organic carbon, respectively; DNH_4 and TNH_4 are dissolved and total ammonium; DKN and TKN are dissolved and total Kjeldahl nitrogen; DP, TP, and DIP are dissolved, total, and dissolved inorganic phosphorus, SpecCond is specific conductivity, and SPM is total suspended matter. The intersite *C*–*Q* slopes for H^+ at humid sites are off scale in (b) and (c): 1.10 ± 0.07 and 0.88 ± 0.07, respectively

humid sites, which changes only slightly when we correct for other site characteristics.

Suspended particulate material (SPM), consistent with its distinct mechanisms of mobilization and transport compared with the other solutes discussed here, exhibits a strong positive slope on both event and interannual timescales but exhibits weak-to-moderate dilution in the intersite comparison, with no significant difference between arid and humid sites. However, if other site characteristics are accounted for, SPM exhibits moderate dilution only for arid sites with no significant effect of discharge for humid sites. Finally, H^+ exhibits a moderate positive slope on both event and interannual timescales, but in the intersite

TABLE 1 Summary of multiple linear regression slope estimates in a backwards-fitting model that minimizes the Bayesian Information Criterion

Parameter	Ca	Mg	Na	K	Sr	Cl	SO_4	F	HCO_3	CO_3	DOC	POC	TOC	NO_2
Intercept	2.297	1.825	2.103	1.654	−0.210	1.869	2.016	0.886	2.938	0.732	2.580	2.133	2.704	−0.067
log_area	**0.053**	**0.049**	**0.068**		*0.056*		**0.102**	**0.040**	**0.049**					
log_slope	**0.142**	**0.106**			**0.222**	**−0.213**		**0.084**			**−0.385**		**−0.283**	**−0.180**
log_dust									**0.363**			*0.477*		**0.507**
Modis_NPP_gC/m^2a (×1,000)			**−0.405**			*−0.338*							*0.199*	
Hijm_T_mean_ann			**0.023**	**0.014**	**0.021**	**0.031**		**0.006**	**−0.020**	**−0.044**				
carbonate=sc+sm	**0.652**	**0.489**	**−0.155**		**0.410**	**0.325**	**0.185**		**0.640**	**0.787**	*−0.112*			**0.119**
magmatic=va+vb+vi+pa+pb+pi+py							**−0.280**	*0.102*				*−0.304*		
mt				**0.214**										**0.226**
ss	**0.297**	**0.312**	**0.167**	**0.087**	**0.286**	**0.222**	**0.365**		**0.210**	**0.589**			*0.115*	
GLC_Artificial	**2.053**	**1.747**	**3.281**	**1.782**		**2.685**	**2.334**	**1.204**	**1.798**	**4.244**		*1.402*		**1.716**
GLC_Managed	**0.493**	**0.823**	**0.735**	**0.462**		**0.741**			**0.618**			**0.873**		**1.023**
GLC_all_forest	*−0.195*			**−0.351**	**−0.608**		**−0.395**	**−0.400**			**0.197**			
GLC_all_water				*−0.439*	*1.039*	*0.799*	**−0.764**	*−0.525*						
humid−arid	**−0.082**	**−0.098**	*−0.080*	**−0.062**	*−0.107*	*−0.004*	**−0.107**	*−0.053*	**−0.123**	**−0.314**	*−0.090*	0.026	*−0.083*	−0.027
arid_log_q	**−0.261**	**−0.305**	**−0.496**	**−0.244**	**−0.452**	**−0.498**	**−0.448**	**−0.209**	**−0.139**	−0.046	−0.081	*−0.318*	**−0.160**	−0.062
humid_log_q	**−0.685**	**−0.797**	*−0.185*	**−0.531**	**−0.425**	*0.023*	**−0.536**	**−0.436**	**−0.457**	*−0.749*	**−0.233**	0.003	**−0.198**	−0.001
Standard error of regression coefficients														
s.e. humid−arid	0.024	0.026	0.029	0.018	0.039	0.038	0.029	0.018	0.024	0.075	0.030	0.054	0.030	0.025
s.e. arid_log_q	0.039	0.042	0.049	0.030	0.061	0.064	0.047	0.028	0.038	0.121	0.055	0.099	0.048	0.041
s.e. humid_log_q	0.051	0.055	0.065	0.038	0.107	0.079	0.061	0.039	0.055	0.227	0.049	0.107	0.059	0.057

Parameter	NO_2&NO_3	DNH4	TNH_4	DKN	DN	TKN	TN	DIP	DP	TP	Spec Cond	SiO_2	SPM	H+
Intercept	1.115	0.569	0.258	1.609	1.256	1.779	1.807	0.228	0.347	0.541	2.100	2.260	1.317	−7.147
log_area		*0.039*	**0.058**	**0.046**	*0.052*						*0.025*		**0.092**	**−0.062**
log_slope		**−0.240**		**−0.331**		**−0.217**			**−0.184**	**0.140**			**0.294**	**−0.482**
log_dust		**0.517**		**0.433**		**0.334**		**0.576**	**0.656**			**0.337**		
Modis_NPP_gC/m^2a (×1,000)				*0.225*	**0.505**		**0.303**		**0.344**				**−0.781**	**0.585**
Hijm_T_mean_ann	**0.012**	*−0.009*		**−0.012**				**0.021**		**0.024**			**0.039**	
carbonate=sc+sm	**0.513**		**−0.208**					*−0.130*		**−0.158**	**0.506**			**−0.880**
magmatic=va+vb+vi+pa+pb+pi+py												**0.333**		**−0.336**
mt	**0.487**	**0.270**	*0.227*			*0.139*								
ss	**0.310**					**0.141**					**0.266**		**0.334**	**−0.316**

(Continues)

TABLE 1 (Continued)

Parameter	NO_2&NO_3	DNH4	TNH_4	DKN	DN	TKN	TN	DIP	DP	TP	Spec Cond	SiO_2	SPM	H+
GLC_Artificial	**1.542**	**2.808**	**1.764**	**1.486**	**2.438**	**0.722**	**2.219**	*1.022*	**3.260**	**1.132**	**1.573**			*−1.101*
GLC_Managed	**1.373**	**0.703**	**1.068**		**1.058**	**0.319**	**0.834**	**0.764**	**0.606**	**0.724**	*0.288*		**1.379**	**−0.877**
GLC_all_forest	*−0.366*			**−0.270**		*−0.189*	*−0.294*	**−0.498**	**−0.432**	**−0.502**	**−0.249**			
GLC_all_water	**−1.382**				*−0.710*		**−1.102**			**−1.579**		**−0.949**	**−2.330**	
humid−arid	0.005	0.009	0.028	−0.010	−0.062	0.011	0.025	−0.061	−0.066	−0.004	*−0.067*	**−0.054**	−0.047	**−0.137**
arid_log_q	−0.007	*−0.124*	−0.125	*−0.115*	−0.022	**−0.237**	**−0.184**	0.046	−0.058	**−0.254**	**−0.379**	−0.044	**−0.326**	0.088
humid_log_q	0.003	0.038	−0.032	−0.055	**−0.346**	**−0.156**	**−0.441**	*−0.235*	*−0.228*	**−0.463**	**−0.493**	**−0.218**	−0.159	**0.786**
Standard error of regression coefficients														
s.e. humid−arid	0.037	0.028	0.033	0.021	0.035	0.019	0.026	0.039	0.032	0.035	0.022	0.014	0.050	0.036
s.e. arid_log_q	0.062	0.048	0.053	0.036	0.057	0.032	0.042	0.067	0.055	0.057	0.036	0.023	0.083	0.059
s.e. humid_log_q	0.077	0.062	0.080	0.051	0.086	0.045	0.056	0.083	0.075	0.071	0.046	0.027	0.119	0.075

Note. The site description terms include an intercept term (to account for any additive offset between humid and arid sites) and log-transformed area (log[km^2]), log-transformed mean topographic slope (log[°]), log-transformed average dust deposition (log[$g{\cdot}m^{-2}{\cdot}year^{-1}$]), MODIS-derived net primary productivity (NPP; $gC{\cdot}m^{-2}{\cdot}year^{-1}$), mean air temperature based on Hijmans et al. (2005; °C), carbonates (%; the sum of the percentage of the watershed area containing either sc (carbonates) or sm (mixed sedimentary) lithologic units), magmatic (%; the sum of the percentage of the watershed area containing va (volcanics, acid), vb (volcanics, basic), vi (volcanics, intermediate), pa (plutonics, acid), pb (plutonics, basic), pi (plutonics, intermediate), or py (pyroclastic) lithologic units), mt (%; the percentage of the watershed area containing metamorphic lithologic units), ss (the percentage of the watershed area containing siliciclastic lithologic units), GLC_Artificial (the proportion of watershed area with urban or manmade cover), GLC_Managed (the proportion of watershed area with agricultural or rangeland cover), GLC_all_forest (the proportion of watershed area with forest cover), GLC_all_water (the proportion of watershed area with open water cover), the proportion of humid and arid sites based on the precipitation threshold of 15 cm $year^{-1}$, and the log-transformed streamflows (log[mm d^{-1}]) for arid and humid sites. If the intercept or streamflow terms were removed in the model fitting procedure, they were manually added back in to evaluate the relationship between analyte concentrations and discharges. Bold font indicates $p < .001$, and italics indicate $p < .01$. If a term was excluded during the backwards-fitting model procedure, then no value is reported, except as noted in section 2 for discharge. Standard errors of regression slope estimates for the discharge terms are also provided at the bottom of the table.

comparison, it exhibits chemostasis across arid sites and a very strong positive slope (0.8 to 1.1, off scale in Figure 3b,c) across humid sites.

Results of the multiple linear regression reveal other subtle controls. Not all potential explanatory variables were statistically meaningful for all solutes, and the resulting models and coefficients are summarized in Table 1. Log-transformed catchment area and dust content were both positively correlated with long-term mean concentrations in all cases where these terms were included in the model, except for the log (area)–[H^+] relationship, which is weakly negative. Because dust is modeled partly from climatic variables, the putative effects of dust may instead reflect the influence of aridity. Dust strongly affects some P and N species. Increases in MODIS-derived net primary productivity are associated with increases in nutrients and decreases in suspended matter, likely due to vegetation inhibiting erosion. Bicarbonate, calcium, and sulfate vary with the abundance of carbonate rocks, as expected, and nitrate also varies with carbonate rock abundance, perhaps due to correlation between agricultural land use and carbonate lithology. Magmatic lithologies were generally weak predictors of solute concentrations, as were metamorphic rocks, except for a possible correlation with some N species, perhaps due to bedrock weathering of N (Holloway & Dahlgren, 2002; Holloway, Dahlgren, Hansen, & Casey, 1998; Houlton, Morford, & Dahlgren, 2018). The abundance of siliciclastic sedimentary rocks was positively correlated with nearly all cations and anions, but it was not a significant predictor of most N and P species. Both managed and artificial (agricultural and urban) land covers are often strongly positively correlated with nearly all analytes. However, interpreting the influence of artificial land cover is statistically challenging because it is so skewed in this data set: Only a handful of urban sites have sufficient data, so a few points can exhibit large leverage. Increases in forest and water cover often lead to decreasing concentrations, as might be expected, especially in anions and most N and P species. In most cases, discharge was an important predictor of solute concentrations, nearly always exhibiting a negative correlation (i.e., dilution behaviour) and often showing a much steeper negative relationship across humid sites than across arid sites (consistent with Figures 2 and 3c). However, NO_2 and TNH_4 exhibited no significant relationship with discharge across either arid or humid sites, and among the N species, only DN, TKN, and TN exhibited significant relationships with discharge across the humid sites.

4 | DISCUSSION

The results presented here show that long-term average weathering-derived solute concentrations vary from catchment to catchment as a function of mean runoff and that on timescales shorter than several years, these solute concentrations in individual catchments vary little from their long-term averages, even during floods or droughts (Figure 3a). The average concentration for a given site and solute can be thought of as a chemical set point, around which geochemical feedbacks act to maintain approximate equilibrium. Expressed in this terminology, the main result presented above is that weathering-derived solute concentrations tend to be quasi-chemostatic, but their set points may vary from catchment to catchment as a function of mean runoff.

We hypothesize that the site-to-site variability in mean solute concentrations as a function of mean runoff serves as a proxy for long-term, climatically driven evolution of these chemical set points for the weathering-derived solutes. (We discuss nutrients and other analytes farther below.) As with any such site-to-site comparison (e.g., Klemes, 1983; Pickett, 1989; Sivapalan, Yaeger, Harman, Xu, & Troch, 2011), the obvious question that arises is whether this proxy is meaningful or not. We can better assess its utility by clarifying two underlying assumptions. First, this interpretation of our results assumes that environmental gradients between sites have remained approximately stationary over months to millennia, the timescales over which weathering reactions can act upon fresh mineral surfaces to promote a quasi-equilibrium between solute production by weathering and solute removal in streamflow. That is, this interpretation does not require that climatic conditions will remain constant but rather that environmental gradients will persist: wetter sites will remain wetter, and drier sites will remain drier, with respect to each other, over long timescales. If this assumption holds, the observed average runoff can be used as a proxy measure, at least in a relative sense, for the wetness conditions under which the critical zones of the different sites have evolved. Using this climosequence, one can interpret site-to-site *C*–*Q* plots like Figure 1c as illustrating how mean solute concentrations respond to different patterns of critical zone evolution under different levels of long-term hydrologic forcing. (This conceptual framework will clearly not apply for analytes driven primarily by stochastic rain chemistry patterns or anthropogenic application of salts or fertilizers.)

Our interpretation also assumes that the climatic differences among the sites are large enough that their effects can be detected despite the confounding influence of lithologic heterogeneity. The multiple regression presented in Table 1 supports this assumption. Although lithologic heterogeneity, especially the abundance of carbonates or siliciclastic sedimentary rocks, may also affect a catchment's set point, discharge is typically a significant predictor of the long-term mean concentration across both arid and humid sites. This result is consistent with climosequence and chronosequence studies that have analysed soil profile development, lysimeter water, and/or catchment-scale streamflow (e.g., Jacobson, Blum, Chamberlain, Poage, & Sloan, 2002; Porder et al., 2007; West et al., 2005). These studies show that large climatic differences may shift set points at millennial timescales but that geochemical set points may also be influenced by lithologic heterogeneity or even large dust inputs.

The patterns observed in the GLORICH data set reflect short-term variations in storage and mobilization of water and solutes, as shaped by the long-term evolution of the critical zone, including soil profile development. The interaction between short-term and long-term variability in weathering-derived solutes reflects the timescale over which the landscape can dampen variability in concentrations, which we can term the typical buffering timescale. We can derive a rough

back-of-the-envelope estimate of typical buffering timescales for weathering-derived solutes, assuming that most of the buffering capacity of the landscape arises from the soil rather than bedrock. This assumption is supported by the fact that both surface area and hydraulic conductivity often decrease exponentially through the soil into the bedrock profile. If cation exchange capacity is approximately 1–10 meq per 100 g (Brady & Weil, 1999) and soils are typically ~1 m deep (e.g., Shangguan, Hengl, Mendes de Jesus, Yuan, & Dai, 2017) with a density of ~1,000 kg m^{-3}, then their exchange capacity is ~10–100 mol m^{-2}. Observed concentrations of weathering-derived solutes in runoff are ~10–1,000 μmol L^{-1} for water yields of ~100–1,000 mm $year^{-1}$ (e.g., Figure 1), implying a chemical denudation rate of ~0.001–1 $mol \cdot m^{-2} \cdot year^{-1}$. Assuming that this chemical flux is derived from the exchange complex, the ratio of the exchange capacity and chemical denudation rate yields an estimated buffering timescale of ~$10–10^5$ years. Thus, where these assumptions hold, one might expect to observe chemostasis at event and interannual timescales (Figure 1a,b and Figure 3a) because these *C*–*Q* patterns arise on timescales much shorter than this characteristic buffering timescale. Over longer timescales, the exchange complex will be unable to buffer solute concentrations in the face of changes in hydrologic forcing, leading to steeper long-term *C*–*Q* relationships for weathering-derived solutes. Thus, if the site-to-site differences in solute concentrations reflect the long-term evolution of the critical zone under different climatic regimes, we would expect site-to-site *C*–*Q* slopes to be steeper than event scale and interannual *C*–*Q* slopes, as observed in Figures 1 and 3, especially for humid sites. This simple back-of-the-envelope analysis is obviously mechanistically incomplete for many solutes, especially those that are not regulated by ion exchange, and is obviously inappropriate for particulate species. Similarly, if most solutes are not derived from unsaturated soil water exchange, this analysis is also inappropriate. Nonetheless, it provides a useful order-of-magnitude estimate for the timescales over which some weathering-derived solutes might be expected to exhibit chemostatic versus non-chemostatic behaviour.

Two factors may account for the fact that many site-to-site *C*–*Q* slopes are steeper across humid sites than across arid sites (Figure 3b, c). First, buffering timescales for arid sites may be longer because the leaching rate is lower (Brady & Weil, 1999). Second, concentrations at arid sites may become high enough that they are regulated by mineral precipitation; thus, at rainfall totals below ~200 mm $year^{-1}$ (Pariente, 2001; exact threshold may vary with temperature), concentrations of many solutes may be held relatively stable by solubility limits.

At each catchment, individual weathering-derived solutes will have their own set points (e.g., Figure 1c), and accurately modeling these differences among solutes may help in understanding how reactions and hydrologic connectivity combine to shape the geochemistry of spatially heterogeneous catchments (e.g., Li et al., 2017; Ocampo, Sivapalan, & Oldham, 2006). The distributions of event and interannual *C*–*Q* slopes also reveal some catchments that deviate from the overall common pattern of chemostasis at short timescales (e.g., the tails of the distributions in Figure 2). These sites might represent exceptions to the expected chemostasis on the basis of the buffering timescale: for example, they may represent sites where human impacts have introduced new solute sources or altered hydrological conditions. Process studies in catchments with unusual *C*–*Q* slopes may lead to process insights that would not be so evident in more typical sites.

Particulates, including SPM and POC, show trends towards more negative slopes at longer timescales, broadly similar to the behaviour observed in weathering-derived solutes. However, in contrast to weathering-derived solutes, SPM and POC exhibit positive slopes at the event and interannual timescales and near-chemostatic or weakly diluting behaviour in site-to-site comparisons. This makes sense because the active controls on particulate and dissolved species differ. At short timescales, particulates are mobilized by floods and not controlled by reaction kinetics. In the intersite comparisons, however, chemostasis or even weakly diluting behaviour (Figure 3b,c) suggests that particulate matter may be somewhat supply limited. Once corrections for other site characteristics are accounted for, particulates' site-to-site slopes are nearly chemostatic across humid sites but are slightly more negative across arid sites (Figure 3c). These comparisons suggest potential interactions between particulate supply limitation and chemical versus physical transport across climatic gradients.

In contrast to both the weathering-derived solutes and particulates, nutrients and most carbon species typically exhibit near-chemostatic behaviour across short and long timescales (Figure 3a,c). Exceptions to this pattern include both carbonate and bicarbonate *C*–*Q* slopes, which exhibit moderate-to-strong dilution-dominated behaviour, especially in the intersite comparison. Multiple regression results show that these *C*–*Q* slopes depend strongly on the abundance of carbonates and the human-managed land cover fraction. Typical near-chemostatic nutrient behaviour is consistent with nutrients being primarily derived from the atmosphere via biogeochemical processes rather than from mineral weathering. Indeed, lithologic differences in this data set are typically not significant predictors of carbon, nitrogen, and phosphorus species (Table 1). Besides carbonates, the main exception to this observation is that the abundance of metamorphic rocks is correlated with the long-term concentrations of several nitrogen species, perhaps consistent with potential lithological sources of nitrogen (Holloway et al., 1998; Holloway & Dahlgren, 2002; Houlton et al., 2018).

The multiple linear regression results (Table 1) also highlight the moderating effect of other site characteristics on most *C*–*Q* relationships, especially across humid sites. In all cases, except for SiO_2, the intersite *C*–*Q* slopes are less steep when site characteristics are accounted for (Figure 3b,c). As noted above, SiO_2 exhibits a consistent chemostatic pattern across all timescales and is well predicted by relatively few terms in the multiple linear regression (Table 1), with the largest weight given to the fraction of the landscape covered by water, followed by stream discharge at humid sites, abundance of magmatic rocks, and dust contributions. We hypothesize that SiO_2 chemostasis may be partially due to trade-offs between biological and dissolved forms that are regulated by complex interactions of biophysical controls; for example, biological Si may be promoted by

warmer temperatures or damped during high flows when SPM concentrations increase, blocking light and thus diatom growth. Lithological controls exhibit a significant influence on 19 of the 28 analytes considered. This observation of broad lithological control is consistent with differences that have been observed among flux–runoff relationships from different lithologies, using event scale flux–discharge data from multiple sites (summarized in Table 4, Bluth & Kump, 1994). These lithological controls might be even more apparent if we had more detailed mineralogical information. For example, in our analysis, all magmatic lithologies are grouped together, even though weathering differences would clearly be expected between basaltic (e.g., Dessert, Dupré, Gaillardet, François, & Allègre, 2003) and granitic (e.g., Oliva et al., 2003) catchments. Furthermore, the prevalence of sedimentary rocks among the GLORICH watersheds may also preclude detailed analysis of lithological controls (following Garrels & Mackenzie, 1967) because the "sedimentary" category includes a wide range of potential minerals available for weathering.

Even with this expanded database and model approach, we cannot explicitly consider many factors that have been suggested as key controls on chemical weathering. This analysis could potentially be extended by assessing changes in weathering surface area at relevant scales (Navarre-Sitchler & Brantley, 2007), surveying mineral composition throughout each watershed (e.g., Gaillardet et al., 1999; Garrels & Mackenzie, 1967), characterizing detailed precipitation chemistry for storm track and evapoconcentration corrections (Négrel, Allègre, Dupré, & Lewin, 1993; Oliva et al., 2003), or measuring distributed erosion rates throughout each watershed (West et al., 2005). Adding this information to the GLORICH database at a global scale would be valuable if it could be derived from measurements rather than models, because model-generated data may simply reflect the model's assumptions and drivers, potentially obscuring real-world patterns.

Our approach here raises a question (that it unfortunately cannot answer): Where do catchments store the solutes that maintain nearly constant concentrations at both high and low flows? One might hypothesize, for example, that nutrients exported during high flow may originate from rapidly decomposing organic material near the soil surface. Assuming that shallow and/or fast flowpaths dominate at high flows, *C*–*Q* relationships may help in distinguishing solutes that are mobilized via these flowpaths (and thus concentrate at high flows) from solutes that are mobilized via deeper and slower flowpaths (and thus dilute at high flows). These different sources and flowpaths have been recognized before (e.g., Anderson et al., 1997; Blumstock, Tetzlaff, Malcolm, Nuetzmann, & Soulsby, 2015; Calmels et al., 2011), often within a single catchment study, and an important next step involves testing these hypothesized sources of solute buffering across many diverse catchments.

18 Nicholas Gubbins

19 Nicholas Gubbins

In the future, it would also be helpful to identify sites that are "hotspots" of highly active weathering, as well as sites where the buffering timescale is expected to be short enough that one could reasonably sample both within and beyond it. This would allow a more direct assessment of the buffering timescale hypothesis outlined in our work. If no real-world catchments can serve this function, the general plausibility of the hypothesis could still be tested in synthetic catchments through virtual experiments with simulation models, on the basis of the interdisciplinary understanding derived from such community efforts as the international critical zone observatory network.

20 Nicholas Gubbins

ACKNOWLEDGMENTS

We thank Suzanne Anderson, Ying Fan, Jeremy Caves, and Anna Radke, as well as two anonymous reviewers, for feedback and discussions that helped to substantially improve this manuscript.

DATA AVAILABILITY STATEMENT

The data that support the findings of this study are summarized in Table S1 and are available from the corresponding author while they are in preparation by J. H. for submission to the Pangaea web portal.

ORCID

Sarah E. Godsey https://orcid.org/0000-0001-6529-7886
Jens Hartmann https://orcid.org/0000-0003-1878-9321
James W. Kirchner https://orcid.org/0000-0001-6577-3619

REFERENCES

Anderson, S. P., Dietrich, W. E., Montgomery, D. R., Torres, R., Conrad, M. E., & Loague, K. (1997). Subsurface flow paths in a steep, unchanneled catchment. *Water Resources Research*, *33*(12), 2637–2653. https://doi.org/10.1063/1.3664967

Arino, O., Gross, D., Ranera, F., Bourg, L., Leroy, M., Bicheron, P., … Weber, J.-L. (2007). GlobCover: ESA service for global land cover from MERIS. In *Geoscience and remote sensing symposium - IGARSS 2007* (pp. 2412–2415). Barcelona, Spain: IEEE International.

Aulenbach, B. T., & Hooper, R. P. (2006). The composite method: An improved method for stream-water solute load estimation. *Hydrological Processes*, *20*(14), 3029–3047. https://doi.org/10.1002/hyp.6147

Basu, N. B., Destouni, G., Jawitz, J. W., Thompson, S. E., Loukinova, N. V., Darracq, A., … Rao, P. S. C. (2010). Nutrient loads exported from managed catchments reveal emergent biogeochemical stationarity. *Geophysical Research Letters*, *37*(23), 1–5. https://doi.org/10.1029/2010GL045168

Berner, R. A., Lasaga, A. C., & Garrels, R. M. (1983). The carbonate-silicate geochemical cycle and its effect on atmospheric carbon dioxide over the past 100 million years. *American Journal of Science*, *283*, 641–683. https://doi.org/10.2475/ajs.283.7.641

Blumstock, M., Tetzlaff, D., Malcolm, I. A., Nuetzmann, G., & Soulsby, C. (2015). Baseflow dynamics: Multi-tracer surveys to assess variable groundwater contributions to montane streams under low flows. *Journal of Hydrology*, *527*, 1021–1033. https://doi.org/10.1016/j.jhydrol.2015.05.019

Bluth, G. J. S., & Kump, L. R. (1994). Lithologic and climatologic controls of river chemistry. *Geochimica et Cosmochimica Acta*, *58*(10), 2341–2359. https://doi.org/10.1016/0016-7037(94)90015-9

Börker, J., Hartmann, J., Romero-Mujalli, G., & Li, G. (2019). Aging of basalt volcanic systems and decreasing CO_2 consumption by weathering. *Earth Surface Dynamics*, *7*, 191–197. https://doi.org/10.5194/esurf-7-191-2019

Brady, N. C., & Weil, R. R. (1999). *The nature and properties of soils* (12th ed.). Harlow, England: Pearson.

Calmels, D., Galy, A., Hovius, N., Bickle, M., West, A. J., Chen, M.-C., & Chapman, H. (2011). Contribution of deep groundwater to the weathering budget in a rapidly eroding mountain belt, Taiwan. *Earth and Planetary Science Letters*, *303*(1–2), 48–58. https://doi.org/10.1016/j.epsl.2010.12.032

Creed, I. F., McKnight, D. M., Pellerin, B. A., Green, M. B., Bergamaschi, B. A., Aiken, G. R., … Stackpoole, S. M. (2015). The river as a chemostat: Fresh perspectives on dissolved organic matter flowing down the river continuum. *Canadian Journal of Fisheries and Aquatic Sciences*, *72*(8), 1272–1285. https://doi.org/10.1139/cjfas-2014-0400

Dessert, C., Dupré, B., Gaillardet, J., François, L. M., & Allègre, C. J. (2003). Basalt weathering laws and the impact of basalt weathering on the global carbon cycle. *Chemical Geology*, *202*(3–4), 257–273. https://doi.org/10.1016/j.chemgeo.2002.10.001

Gaillardet, J., Dupre, B., Louvat, P., & Allegre, C. J. (1999). Global silicate weathering and CO_2 consumption rates from the chemistry of large rivers. *Chemical Geology*, *159*, 3–30. https://doi.org/10.1016/S0009-2541(99)00031-5

Garrels, R. M., & Mackenzie, F. T. (1967). Origin of the chemical compositions of some springs and lakes. In *Equilibrium concepts in natural water systems* (pp. 222–242). Advances in Chemistry Series 67. Washington, DC: American Chemical Society. https://doi.org/10.1021/ba-1967-0067.ch010

Godsey, S. E., Kirchner, J. W., & Clow, D. W. (2009). Concentration-discharge relationships reflect chemostatic characteristics of US catchments. *Hydrological Processes*, *23*, 1844–1864. https://doi.org/10.1002/hyp.7315

Hale, R. L., & Godsey, S. E. (2019). Dynamic stream network intermittence explains emergent dissolved organic carbon chemostasis in headwaters. *Hydrological Processes*, *33*(13), 1926–1936. https://doi.org/10.1002/hyp.13455

Hall, F. R. (1970). Dissolved solids-discharge relationships: 1. Mixing models. *Water Resources Research*, *6*(3), 845–850. https://doi.org/10.1029/WR006i003p00845

Hartmann, J., Lauerwald, R., & Moosdorf, N. (2014). A brief overview of the GLObal RIver Chemistry Database, GLORICH. *Procedia Earth and Planetary Science*, *10*, 23–27. https://doi.org/10.1016/j.proeps.2014.08.005

Hartmann, J., & Moosdorf, N. (2012). The new global lithological map database GLiM: A representation of rock properties at the Earth surface. *Geochemistry, Geophysics, Geosystems*, *13*(12), 1–37. https://doi.org/10.1029/2012GC004370

Hem, D. (1985). Study and interpretation the chemical of natural of characteristics water. USGS Water Supply Paper 2254 (Vol. 2254). Alexandria, VA. Retrieved from http://pubs.usgs.gov/wsp/wsp2254/pdf/wsp2254a.pdf

Herndon, E. M., Dere, A. L., Sullivan, P. L., Norris, D., Reynolds, B., & Brantley, S. L. (2015). Biotic controls on solute distribution and transport in headwater catchments. *Hydrology and Earth System Sciences Discussions*, *12*(1), 213–243. https://doi.org/10.5194/hessd-12-213-2015

Hijmans, R. J., Cameron, S. E., Parra, J. L., Jones, P. G., & Jarvis, A. (2005). Very high resolution interpolated climate surfaces for global land areas. *International Journal of Climatology*, *25*(15), 1965–1978. https://doi.org/10.1002/joc.1276

Hilley, G. E., & Porder, S. (2008). A framework for predicting global silicate weathering and CO_2 drawdown rates over geologic time-scales. *Proceedings of the National Academy of Sciences*, *105*(44), 16855–16859. https://doi.org/10.1073/pnas.0801462105

Holloway, J. M., & Dahlgren, R. A. (2002). Nitrogen in rock: Occurrences and biogeochemical implications. *Global Biogeochemical Cycles*, *16*(4), 65-1–65–17. https://doi.org/10.1029/2002gb001862

Holloway, J. M., Dahlgren, R. A., Hansen, B., & Casey, W. H. (1998). Contribution of bedrock nitrogen to high nitrate concentrations in stream water. *Nature*, *395*(October), 785–788. https://doi.org/10.1038/27410

Houlton, B. Z., Morford, S. L., & Dahlgren, R. A. (2018). Convergent evidence for widespread rock nitrogen sources in Earth's surface environment. *Science*, *360*(6384), 58–62. https://doi.org/10.1126/science.aan4399

House, W. A., & Warwick, M. S. (1998). Hysteresis of the solute concentration/discharge relationship in rivers during storms. *Water Research*, *32*(8), 2279–2290. https://doi.org/10.1016/S0043-1354(97)00473-9

Ibarra, D. E., Caves, J. K., Moon, S., Thomas, D. L., Hartmann, J., Chamberlain, C. P., & Maher, K. (2016). Differential weathering of basaltic and granitic catchments from concentration–discharge relationships. *Geochimica et Cosmochimica Acta*, *190*, 265–293. https://doi.org/10.1016/j.gca.2016.07.006

Ibarra, D. E., Moon, S., Caves, J. K., Chamberlain, C. P., & Maher, K. (2017). Concentration–discharge patterns of weathering products from global rivers. *Acta Geochimica*, *36*(3), 405–409. https://doi.org/10.1007/s11631-017-0177-z

Jacobson, A. D., Blum, J. D., Chamberlain, C. P., Poage, M. A., & Sloan, V. F. (2002). Ca/Sr and Sr isotope systematics of a Himalayan glacial chronosequence: Carbonate versus silicate weathering rates as a function of landscape surface age. *Geochimica et Cosmochimica Acta*, *66*(1), 13–27. https://doi.org/10.1016/S0016-7037(01)00755-4

Johnson, N., Likens, G., Bormann, F. H., Fisher, D., & Pierce, R. S. (1969). A working model for the variation in stream water chemistry at the Hubbard Brook Experimental Forest, New Hampshire. *Water Resources Research*, *5*(6), 1353–1363. https://doi.org/10.1029/WR005i006p01353

Klemes, V. (1983). Conceptualization and scale in hydrology. *Journal of Hydrology*, *65*(1–3), 1–23. https://doi.org/10.1016/0022-1694(83)90208-1

Kump, L. R., Brantley, S. L., & Arthur, M. A. (2000). Chemical weathering, atmospheric CO_2, and climate. *Annual Review of Earth and Planetary Sciences*, *28*, 611–667. https://doi.org/10.1146/annurev.earth.28.1.611

Li, L., Bao, C., Sullivan, P. L., Brantley, S., Shi, Y., & Duffy, C. (2017). Understanding watershed hydrogeochemisty: 2. Synchronized hydrological and geochemical processes drive stream chemostatic behavior. *Water Resources Research*, *53*, 2346–2367. https://doi.org/10.1002/2016WR019676.Received

Lloyd, C. E. M., Freer, J. E., Johnes, P. J., & Collins, A. L. (2016a). Technical note: Testing an improved index for analysing storm discharge-concentration hysteresis. *Hydrology and Earth System Sciences*, *20*(2), 625–632. https://doi.org/10.5194/hess-20-625-2016

Lloyd, C. E. M., Freer, J. E., Johnes, P. J., & Collins, A. L. (2016b). Using hysteresis analysis of high-resolution water quality monitoring data, including uncertainty, to infer controls on nutrient and sediment transfer in catchments. *Science of the Total Environment*, *543*(November 2015), 388–404. https://doi.org/10.1016/j.scitotenv.2015.11.028

Maher, K. (2011). The role of fluid residence time and topographic scales in determining chemical fluxes from landscapes. *Earth and Planetary Science Letters*, *312*(1–2), 48–58. https://doi.org/10.1016/j.epsl.2011.09.040

Maher, K., & Chamberlain, C. P. (2014). Hydrologic regulation of chemical weathering and the geologic. *Science*, *343*(6178), 1502–1504. https://doi.org/10.1126/science.1250770

Mahowald, N. M., Baker, A. R., Bergametti, G., Brooks, N., Duce, R. A., Jickells, T. D., … Tegen, I. (2005). Atmospheric global dust cycle and iron inputs to the ocean. *Global Biogeochemical Cycles*, *19*(4), GB4025. https://doi.org/10.1029/2004GB002402

Meybeck, M. (1987). Global chemical weathering of surficial rocks estimated from river dissolved loads. *American Journal of Science*, *287*, 401–428. https://doi.org/10.2475/ajs.287.5.401

Moatar, F., Abbott, B., Minaudo, C., Curie, F., & Pinay, G. (2017). Elemental properties, hydrology, and biology interact to shape concentration-discharge curves for carbon, nutrients, sediment, and major ions. *Water Resources Research*, *53*, 1270–1287. https://doi.org/10.1002/2016WR019676.Received

Moon, S., Chamberlain, C. P., & Hilley, G. E. (2014). New estimates of silicate weathering rates and their uncertainties in global rivers. *Geochimica et Cosmochimica Acta*, *134*, 257–274. https://doi.org/10.1016/j.gca.2014.02.033

Musolff, A., Fleckenstein, J. H., Rao, P. S. C., & Jawitz, J. W. (2017). Emergent archetype patterns of coupled hydrologic and biogeochemical responses in catchments. *Geophysical Research Letters*, *44*(9), 4143–4151. https://doi.org/10.1002/2017GL072630

Navarre-Sitchler, A., & Brantley, S. (2007). Basalt weathering across scales. *Earth and Planetary Science Letters*, *261*(1–2), 321–334. https://doi.org/10.1016/j.epsl.2007.07.010

Négrel, P., Allègre, C. J., Dupré, B., & Lewin, E. (1993). Erosion sources determined by inversion of major and trace element ratios and strontium isotopic ratios in river water: The Congo Basin case. *Earth and Planetary Science Letters*, *120*(1–2), 59–76. https://doi.org/10.1016/0012-821X(93)90023-3

Ocampo, C. J., Sivapalan, M., & Oldham, C. (2006). Hydrological connectivity of upland-riparian zones in agricultural catchments: Implications for runoff generation and nitrate transport. *Journal of Hydrology*, *331*(3–4), 643–658. https://doi.org/10.1016/j.jhydrol.2006.06.010

Oliva, P., Viers, J., & Dupré, B. (2003). Chemical weathering in granitic environments. *Chemical Geology*, *202*(3–4), 225–256. https://doi.org/10.1016/j.chemgeo.2002.08.001

Oudin, L., Andreassian, V., Perrin, C., Michel, C., & Le Moine, N. (2008). Spatial proximity, physical similarity, regression and ungaged catchments: A comparison of regionalization approaches based on 913 French catchments. *Water Resources Research*, *44*(3), 1–15. https://doi.org/10.1029/2007WR006240

Pariente, S. (2001). Soluble salts dynamics in the soil under different climatic conditions. *Catena*, *43*, 307–321. https://doi.org/10.1016/S0341-8162(00)00130-2

Pickett, S. T. A. (1989). Long-term studies in ecology. In G. E. Likens (Ed.), *Long-term studies in ecology: Approaches and alternatives* (pp. 110–135). New York: Springer-Verlag New York. https://doi.org/10.1007/978-1-4615-7358-6_5

Pinder, G. F., & Jones, J. F. (1969). Determination of the ground-water component of peak discharge from the chemistry of total runoff. *Water Resources Research*, *5*(2), 438–445. https://doi.org/10.1029/WR005i002p00438

Porder, S., Hilley, G. E., & Chadwick, O. A. (2007). Chemical weathering, mass loss, and dust inputs across a climate by time matrix in the Hawaiian Islands. *Earth and Planetary Science Letters*, *258*(3–4), 414–427. https://doi.org/10.1016/j.epsl.2007.03.047

Rose, L. A., Karwan, D. L., & Godsey, S. E. (2018). Concentration–discharge relationships describe solute and sediment mobilization, reaction, and transport at event and longer timescales. *Hydrological Processes*, *32*(18), 2829–2844. https://doi.org/10.1002/hyp.13235

Shangguan, W., Hengl, T., Mendes de Jesus, J., Yuan, H., & Dai, Y. (2017). Mapping the global depth to bedrock for land surface modeling. *Journal of Advances in Modeling Earth Systems*, *9*, 65–88. https://doi.org/10.1002/2016MS000686

Sivapalan, M., Yaeger, M. A., Harman, C. J., Xu, X., & Troch, P. A. (2011). Functional model of water balance variability at the catchment scale: 1. Evidence of hydrologic similarity and space-time symmetry. *Water Resources Research*, *47*(2), 1–18. https://doi.org/10.1029/2010WR009568

Stallard, R. F., & Murphy, S. F. (2014). A unified assessment of hydrologic and biogeochemical responses in research watersheds in eastern Puerto Rico using runoff-concentration relations. *Aquatic Geochemistry*, *20*(2–3), 115–139. https://doi.org/10.1007/s10498-013-9216-5

Tardy, Y., Bustillo, V., & Boeglin, J. L. (2004). Geochemistry applied to the watershed survey: Hydrograph separation, erosion and soil dynamics. A case study: The basin of the Niger River, Africa. *Applied Geochemistry*, *19*(4), 469–518. https://doi.org/10.1016/j.apgeochem.2003.07.003

Taylor, A., & Blum, J. D. (1995). Relation between soil age and silicate weathering rates determined from the chemical evolution of a glacial chronosequence. *Geology*, *23*(11), 979–982. https://doi.org/10.1130/0091-7613(1995)023<0979:RBSAAS>2.3.CO;2

Walling, D. E., & Webb, B. W. (1986). Solutes in river systems. In S. T. Trudgill (Ed.), *Solute Processes* (pp. 251–327). Chichester: John Wiley and Sons.

West, A. J., Galy, A., & Bickle, M. (2005). Tectonic and climatic controls on silicate weathering. *Earth and Planetary Science Letters*, *235*(1–2), 211–228. https://doi.org/10.1016/j.epsl.2005.03.020

White, A. F., & Blum, A. E. (1995). Effects of climate on chemical weathering in watersheds. *Geochimica et Cosmochimica Acta*, *59*(9), 1729–1747. https://doi.org/10.1016/0016-7037(95)00078-E

White, A. F., Blum, A. E., Schulz, M. S., Bullen, T. D., Harden, J. W., & Peterson, M. L. (1996). Chemical weathering of a soil chronosequence on granite alluvium I. Reaction rates based on changes in soil mineralogy. *Geochimica et Cosmochimica Acta*, *60*(14), 2533–2550. https://doi.org/10.1016/0016-7037(96)00106-8

Zhao, M., Heinsch, F. A., Nemani, R. R., & Running, S. W. (2005). Improvements of the MODIS terrestrial gross and net primary production global data set. *Remote Sensing of Environment*, *95*(2), 164–176. https://doi.org/10.1016/j.rse.2004.12.011

SUPPORTING INFORMATION

Additional supporting information may be found online in the Supporting Information section at the end of this article.

How to cite this article: Godsey SE, Hartmann J, Kirchner JW. Catchment chemostasis revisited: Water quality responds differently to variations in weather and climate. *Hydrological Processes*. 2019;33:3056–3069. https://doi.org/10.1002/hyp.13554

Catchment chemostasis revisited: Water quality responds differently to variations in weather and climate

Godsey, Sarah E.; Hartmann, Jens; Kirchner, James W.

01 Nicholas Gubbins Page 1
8/7/2021 17:54

02 Nicholas Gubbins Page 1
8/7/2021 18:29

03 Nicholas Gubbins Page 3
8/7/2021 18:36

04 Nicholas Gubbins Page 3
8/7/2021 18:36

05 Nicholas Gubbins Page 4
8/7/2021 18:41

06 Nicholas Gubbins Page 4
8/7/2021 18:41

07 Nicholas Gubbins Page 4
8/7/2021 22:41

08 Nicholas Gubbins Page 4
8/7/2021 18:44

09 Nicholas Gubbins Page 5
8/7/2021 18:49

10 Nicholas Gubbins Page 10

8/7/2021 22:41

11 Nicholas Gubbins Page 10

8/7/2021 22:42

12 Nicholas Gubbins Page 10

8/7/2021 22:42

13 Nicholas Gubbins Page 10

8/7/2021 22:42

14 Nicholas Gubbins Page 10

8/7/2021 22:43

15 Nicholas Gubbins Page 10

8/7/2021 22:43

16 Nicholas Gubbins Page 10

8/7/2021 21:14

17 Nicholas Gubbins Page 10

8/7/2021 21:12

18 Nicholas Gubbins Page 12

8/7/2021 22:01

19 Nicholas Gubbins Page 12

8/7/2021 22:02

20 Nicholas Gubbins Page 12

8/7/2021 22:03